Cell Reports
Medicine

Article

Discovery, delineation, and therapeutic targeting of a hyper-translation pathway driving cytokine release syndrome

Graphical abstract

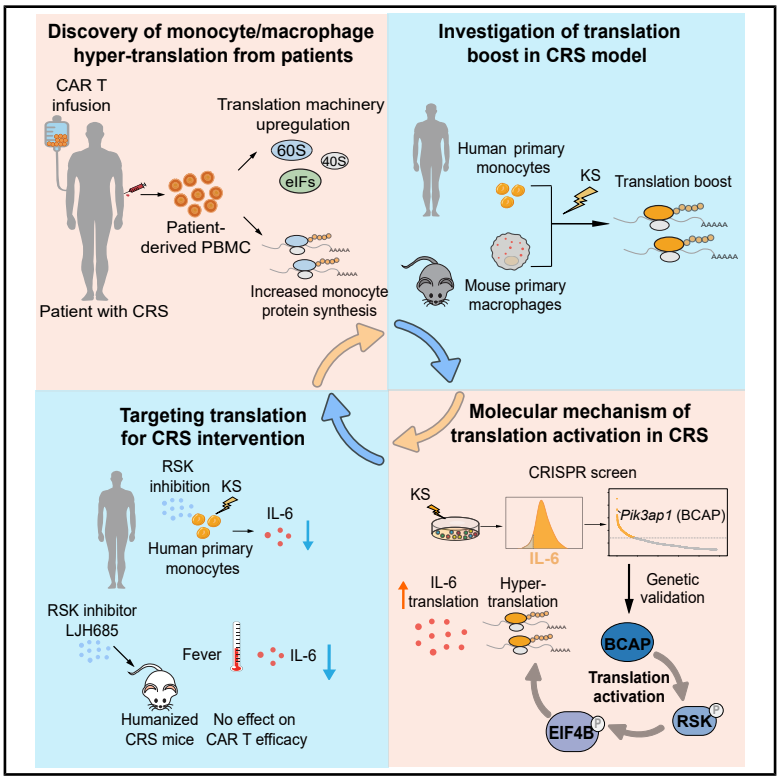

Highlights

- Monocyte/macrophage hyper-translation is a hallmark of cytokine release syndrome (CRS)
- Monocyte/macrophage hyper-translation boosts IL-6 production and promotes CRS
- BCAP-RSK-EIF4B axis drives monocyte/macrophage hyper-translation in CRS
- Targeting hyper-translation represents a potential therapeutic strategy for CRS

Authors

Xingxian Liu, Jiaqi Li, Yajing Zhang, ..., Deng Pan, Weidong Han, Xiaoyu Hu

Correspondence

hanwdrsw@163.com (W.H.), huxiaoyu@westlake.edu.cn (X.H.)

In brief

Liu et al. discover monocyte/macrophage hyper-translation in patients with cytokine release syndrome (CRS), define its molecular mechanism, and demonstrate that targeting hyper-translation can serve as a therapeutic approach for CRS.

Liu et al., 2026, Cell Reports Medicine 7, 102531
January 20, 2026
https://doi.org/10.1016/j.xcrm.2025.102531

CellPress

Cell Reports Medicine

CellPress
OPEN ACCESS

Article

Discovery, delineation, and therapeutic targeting of a hyper-translation pathway driving cytokine release syndrome

Xingxian Liu,[1,2,3,10] Jiaqi Li,[1,2,3,10] Yajing Zhang,[4,5] Yang Liu,[4] Chunmeng Wang,[4] Yao Wang,[4] Yunqi Liu,[1,2,3] Yuzhuo Yang,[1,2,3] Yao Su,[6] Youxue Lu,[2,3] Wenyan Wang,[2,7] Yang-Xin Fu,[2,7] Xin Lin,[1,2,3] Deng Pan,[2,3] Weidong Han,[4,*] and Xiaoyu Hu[8,9,11,*]

[1]Institute for Immunology, Tsinghua University, Beijing, China
[2]School of Basic Medical Sciences, Tsinghua University, Beijing, China
[3]Tsinghua-Peking Center for Life Sciences, Beijing, China
[4]Department of Bio-therapeutic, the First Medical Center, Chinese PLA General Hospital, Beijing, China
[5]Department of Myeloma and Lymphoma, Beijing GoBroad Boren Hospital, GoBroad Medical Institute of Hematology (Beijing Center), Beijing, China
[6]National Protein Science Facility, School of Life Science, Tsinghua University, Beijing, China
[7]State Key Laboratory of Molecular Oncology, Tsinghua University, Beijing, China
[8]Westlake University School of Medicine, Hangzhou, China
[9]Westlake University School of Medicine-affiliated Hangzhou First People's Hospital, Hangzhou, China
[10]These authors contributed equally
[11]Lead contact
*Correspondence: hanwdrsw@163.com (W.H.), huxiaoyu@westlake.edu.cn (X.H.)
https://doi.org/10.1016/j.xcrm.2025.102531

SUMMARY

Cytokine release syndrome (CRS) is a potentially life-threatening inflammatory condition. However, the defining features that distinguish it from self-resolving inflammation remain poorly understood. In this study, we identified monocyte/macrophage hyper-translation as a hallmark of CRS pathogenesis in patient samples. To uncover the molecular drivers of this phenomenon, a CRISPR screen followed by genetic validation pinpointed BCAP as a critical regulator of hyper-translation. Mechanistically, BCAP activated the RSK-EIF4B axis, fueling hyperactive translation in macrophages. Genetic ablation of RSK attenuated CRS-associated inflammation, and pharmacological inhibition of RSK alleviated CRS symptoms in a humanized mouse model. These findings establish hyper-translation as a key pathogenic feature of CRS and highlight protein translation as a druggable pathway, opening venues for therapeutic interventions of CRS and other inflammatory diseases.

INTRODUCTION

Inflammation is a fundamental physiological process essential for survival, underpinning a wide range of biological functions, including but not limited to organismal development, immune defense, tissue remodeling, and metabolic adaptation.[1–3] To maintain homeostasis, inflammation is typically self-limiting and resolvable, fulfilling its necessary functions without causing excessive tissue damage.[4–6] However, not all inflammatory responses properly resolve. Uncontrolled and non-resolvable inflammation underlies pathogenesis of numerous human diseases, such as autoimmune diseases and metabolic disorders.[7] One extreme manifestation of uncontrolled inflammation takes the form of cytokine release syndrome (CRS), which is commonly triggered by infections or immunotherapies.[8–10] It is estimated that 50%–90% patients receiving chimeric antigen receptor (CAR) T cell therapy develop CRS, with clinical manifestations ranging from mild fever to life-threatening multiorgan failure.[8–10] At the core of CRS pathogenesis is the excessive production of pro-inflammatory cytokines, most notably interleukin-6 (IL-6).[8,9] Monocytes and macrophages serve as major producers of inflammatory mediators and cellular drivers of this cytokine storm.[11,12] While CRS shares key effector molecules, such as IL-6, with classic resolvable inflammation, it is distinguished by the unusually heightened magnitude and distinct temporal dynamics of cytokine release, leading to sustained and often deleterious systemic inflammation.[9] Although recent research has begun to shed light on pathways contributing to the excessive cytokine production observed in CRS,[13] the precise mechanisms fueling uncontrolled inflammation and thus distinguishing CRS from other inflammatory conditions remain incompletely understood.

The transcriptional production of mRNAs encoding key inflammatory mediators has long been regarded as the rate-limiting step in shaping inflammatory responses,[14] dominating research efforts in the field. In the canonical model of macrophage-mediated inflammation, microbial signals such as lipopolysaccharide

Please cite this article in press as: Liu et al., Discovery, delineation, and therapeutic targeting of a hyper-translation pathway driving cytokine release syndrome, Cell Reports Medicine (2025), https://doi.org/10.1016/j.xcrm.2025.102531

(LPS) initiate intracellular signaling cascades that culminate in DNA-bound transcription factors activating inflammatory gene expression.[14,15] Although significant advances have been made in understanding the regulation of protein translation,[16,17] its specific role in controlling innate immunity, especially in human inflammatory disease setting, remains understudied.[18,19] In fact, translation is a metabolically demanding process, accounting for nearly 50% of a mammalian cell's total energy consumption.[20] Such resource intensity strongly suggests that translation might operate in tandem with transcription as an actively regulated checkpoint in inflammation. Since many key inflammatory mediators function as peptides, the ultimate impact of inflammation hinges on the combined contributions of transcriptional and translational regulation.[18,19,21] While inflammation has been extensively studied through the lens of transcriptional control, with well-defined signaling pathways connecting upstream stimuli with downstream inflammatory gene transcription,[14] translational regulation along with its therapeutic potential remain underexplored.

Recently, inspired by a serendipitous clinical event, we discovered that metoprolol, a β1-adrenergic receptor blocker, partially alleviates CRS severity in patients undergoing CAR T therapies by lowering IL-6 production. Surprisingly, subsequent mechanistic investigations revealed that metoprolol does not alter *IL6* gene transcription. Instead, it attenuates the translation efficiency (TE) of IL-6 in human monocytes and macrophages, leading to reduced IL-6 protein despite comparable levels of *IL6* mRNA transcripts.[22] These findings provide hints that the translation of key inflammatory mediators represents a pivotal step in CRS pathogenesis. To comprehensively elucidate CRS pathogenesis in a clinically relevant context, we analyzed inflammatory signatures in patients with CRS. Our analyses revealed that macrophages/monocytes from these patients consistently exhibit features of hyper-translation, termed monocyte/macrophage hyper-translation (MHT). MHT amplifies IL-6 production and exacerbates disease severity. By integrating CRISPR screening, multi-omics approaches, and genetic validation, we identified a core signaling pathway driving MHT. Pharmacological inhibition of this pathway markedly attenuated CRS symptoms in a humanized mouse model without compromising CAR T efficacy, establishing MHT as both a hallmark of CRS pathogenesis and a promising therapeutic target.

RESULTS

Monocyte/macrophage hyper-translation is a hallmark of human CRS

To characterize the inflammatory signatures of human CRS, we isolated peripheral blood mononuclear cells (PBMCs) from patients with refractory/relapsed B cell lymphoma or multiple myeloma undergoing CAR T therapy (Figure S1A). Samples were collected at pre-infusion and post-infusion stage, as indicated by fever and elevated serum IL-6 levels (Figures 1A and S1B). Mass spectrometry analysis of paired samples from CAR T-treated patients revealed profound proteomics alterations during CRS (Figure S1C). Notably, the most prominently upregulated protein clusters were associated with the translation process (Figure 1B). These clusters included key components of the translation machinery, such as eukaryotic initiation factors (EIFs), RNA-binding proteins, and ribosomal proteins of the 40S (RPSs) and 60S (RPLs) subunits (Figure 1C). Given the established role of monocytes and macrophages in CRS pathogenesis,[11,12] we further monitored translational activity of monocytes from patients with CRS using the surface sensing of translation (SUnSET) technique[23] by assessing puromycin incorporation as a measurement for protein synthesis and translation rates (Figure 1D). At the post-infusion stage, $CD14^+$ monocytes exhibited markedly increased puromycin incorporation (Figure 1D), showing enhanced translation activity during CRS progression.

To conduct in-depth investigations of the observed hyper-translation in patients, we utilized a previously described model system closely recapitulating the features of human CRS,[22] in which primary monocytes were cultured with CAR T killing supernatant (KS) (Figures 1E and S1D). Consistent with the hyper-translation in patients, KS-stimulated human monocytes exhibited robust puromycin incorporation (Figure 1E), indicating a significant elevation in translational activity. In contrast, LPS stimulation resulted in only weak puromycin incorporation, demonstrating that the observed translation enhancement is more specific to CRS (Figure 1E). To delineate the monocyte translational landscape in CRS, we employed ribosome profiling (Ribo-seq)[24,25] and calculated TE by comparing ribosome-protected fragments (RPFs) with mRNA abundance (Figure 1F). Translatome analysis revealed a prominent increase in TE under the CRS condition (Figures 1F and 1G). Gene-wise TE distribution closely correlated with RPF signals, but not with mRNA levels, corroborating a translation-dominant regulatory pattern (Figure 1G). Intriguingly, approximately one-third of protein-coding genes in monocytes were translationally upregulated during CRS (Figures 1H and S1E), with a significant enrichment in translation-related genes (Figure 1I). Protein upregulation of several translation-related genes, including ribosomal components RPLP0 and RPS3 and EIF2A and EIF4B, was validated (Figure 1J), as well as several additional genes (Figure S1F). Collectively, these results establish MHT as a hallmark of human CRS.

Translatome alterations predominantly associate with CRS rather than canonical inflammation

To enable genetic manipulations, we developed a murine cell-based system in which wild-type C57/B6J mouse T cells were transduced with an anti-EGFR (epidermal growth factor receptor) CAR and co-cultured with EGFR-overexpressing B16 tumor cells. The resulting KS was then used to stimulate mouse bone marrow-derived macrophages (BMDMs), eliciting IL-6 production kinetics similar to those observed in the human KS system (Figures 2A and S2A). Polysome fractionation analysis of BMDMs revealed an increase in mRNA-bound ribosome components, accompanied by a concomitant reduction in free messenger ribonucleoprotein particles (mRNPs) following KS stimulation (Figure 2B). These results indicate that murine macrophages undergo a hyper-translation event comparable to that seen in human CRS, establishing this model as a suitable system for subsequent mechanistic investigations.

To comprehensively profile the translatome in CRS, we employed a myeloid-specific RiboTag-seq strategy.[26] This

Please cite this article in press as: Liu et al., Discovery, delineation, and therapeutic targeting of a hyper-translation pathway driving cytokine release syndrome, Cell Reports Medicine (2025), https://doi.org/10.1016/j.xcrm.2025.102531

CellPress
OPEN ACCESS

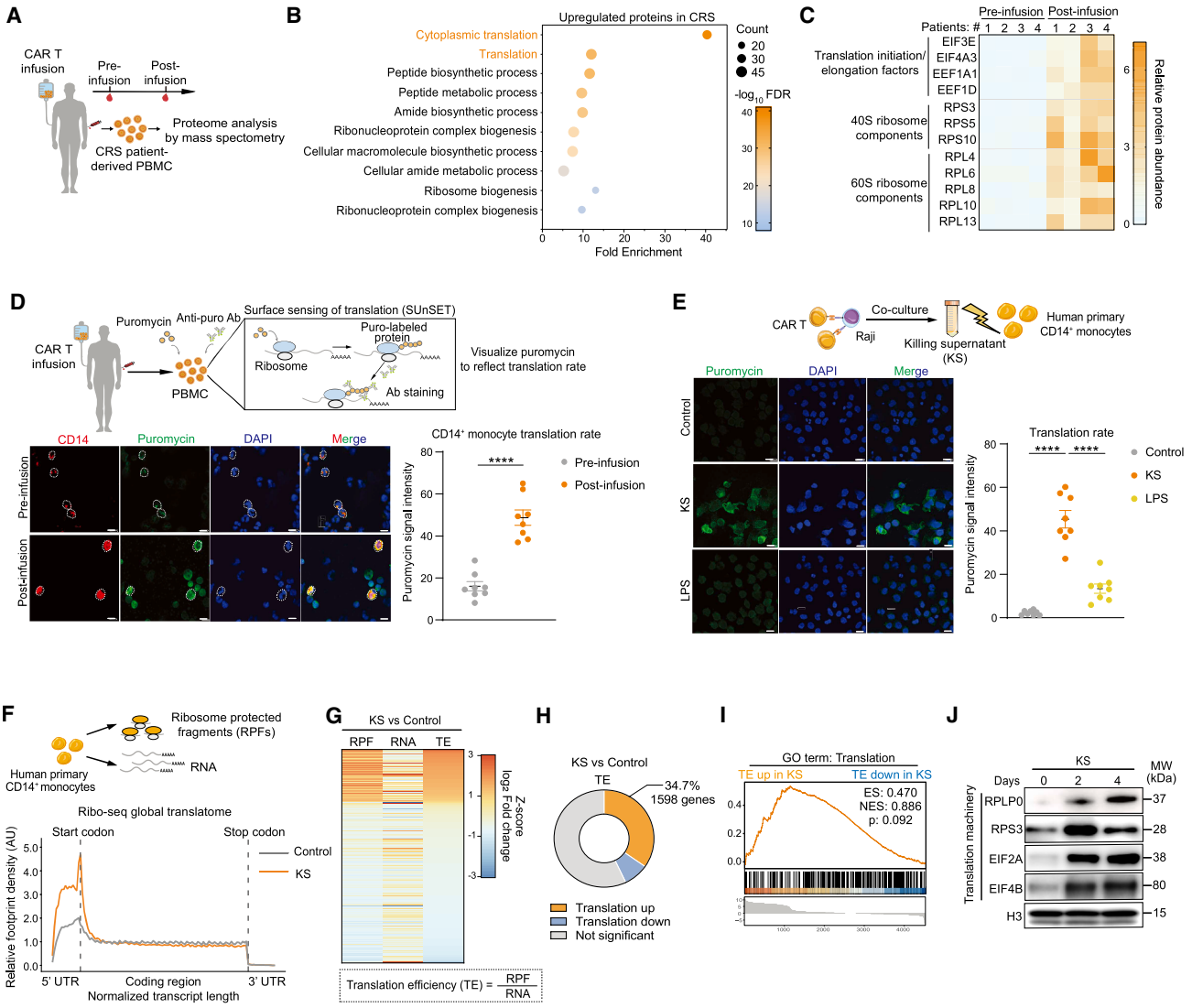

Figure 1. Monocyte/macrophage hyper-translation is a hallmark of human CRS

(A) Schematic representation of proteome analysis performed on PBMCs derived from patients with CRS at pre- and post-infusion.

(B) Gene Ontology (GO) analysis of upregulated proteins in PBMCs from four patients at post-infusion.

(C) Heatmap displaying highly upregulated proteins associated with the GO term "Cytoplasmic translation" at post-infusion.

(D) Schematic of the SUnSET assay and puromycin incorporation in PBMCs from patients (upper). Representative immunofluorescence images showing puromycin (green) incorporation in $CD14^+$ monocytes (red); nuclei were stained with DAPI (blue). Scale bars, 10 μm (lower left). Quantification of puromycin intensity in $CD14^+$ monocytes (lower right). Fluorescence intensity was measured from 8 representative images of $CD14^+$ monocytes from three patients.

(E) Schematic of the *in vitro* KS system with human monocytes (upper). Representative images showing puromycin (green) incorporation in monocytes stimulated with KS (120 h) or LPS (6 h); nuclei were stained with DAPI (blue). Scale bars, 10 μm (lower left). Translation rate quantitated by puromycin intensity is shown (lower right). Fluorescent intensity was quantitated of 8 representative images from three independent experiments. Data are presented as mean ± SEM in (D and E); $^{****}p < 0.0001$, unpaired *t* test.

(F) Schematic of ribosome profiling (Ribo-seq) in KS-stimulated monocytes (upper). Metagene analyses of ribosome footprints aligned to normalized transcript in KS-stimulated (120 h) and control monocytes. Dashed lines indicate start codon and stop codon (lower).

(G) Heatmap of RPF, RNA, and TE in KS-stimulated monocytes from Ribo-seq.

(H) Schematic of translation boost in KS-stimulated monocytes by Ribo-seq TE analysis.

(I) Gene set enrichment analysis (GSEA) of TE in KS-stimulated monocytes by GO term "Translation".

(J) Western blot analysis of translation machinery in KS-stimulated monocytes. Histone protein H3 was used as a loading control. Representative data of three independent experiments.

Please cite this article in press as: Liu et al., Discovery, delineation, and therapeutic targeting of a hyper-translation pathway driving cytokine release syndrome, Cell Reports Medicine (2025), https://doi.org/10.1016/j.xcrm.2025.102531

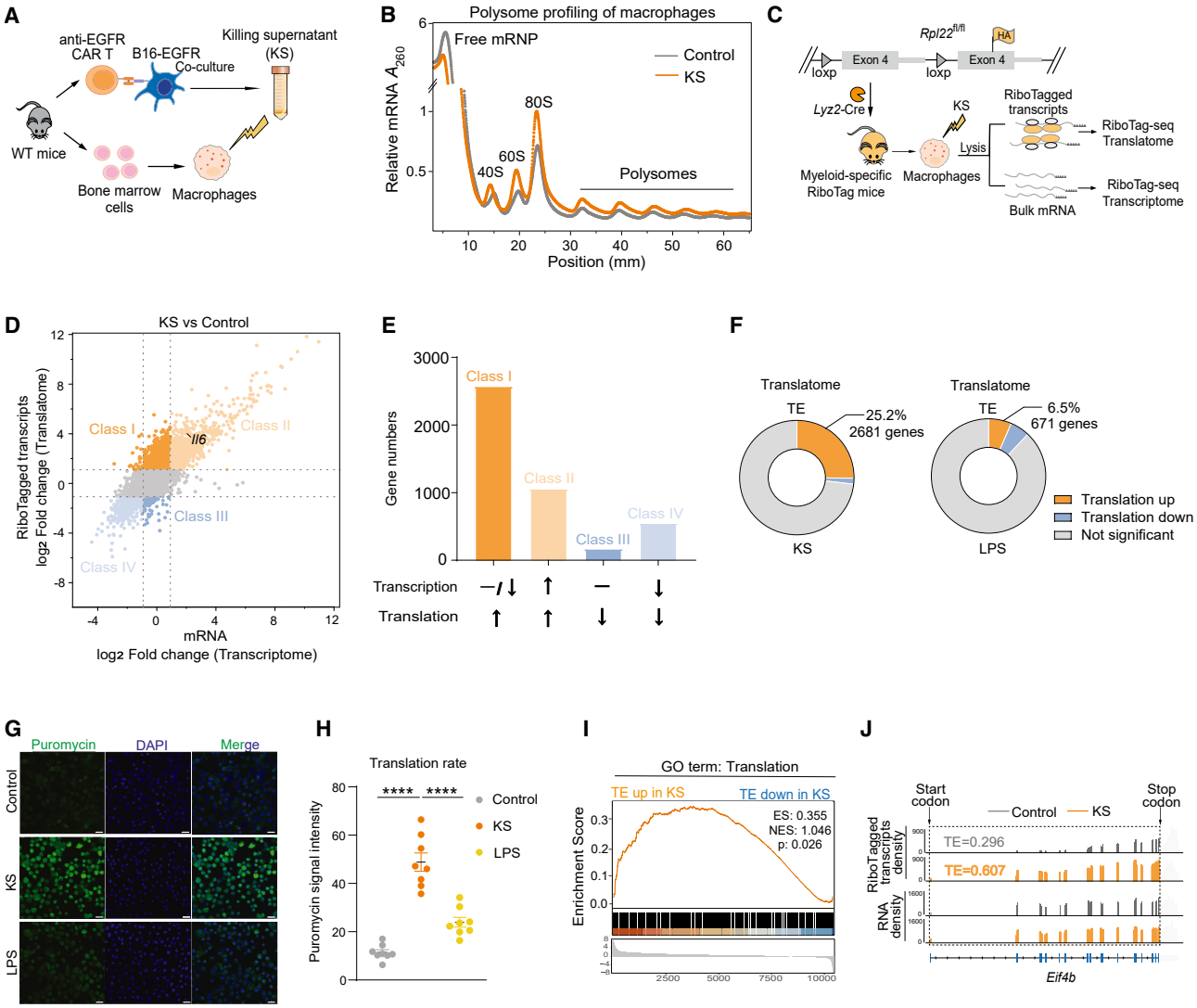

Figure 2. CRS is predominantly associated with translatome changes

(A) Schematic of the *in vitro* KS system with mouse BMDMs.

(B) Polysome profiling of BMDMs stimulated with KS (24 h) versus control. The peaks corresponding to free mRNP, 40S, 60S, 80S, and polysome were marked on top. A_{260} absorbance was normalized to 80S peak value of the KS group.

(C) Schematic of the RiboTag-seq of KS-stimulated BMDMs.

(D and E) Scatterplot comparing translatome versus transcriptome of KS-stimulated BMDMs from RiboTag-seq. Genes were divided into 4 groups based on changes in transcriptome and translatome, as shown in (E).

(F) Schematic of translation activation in KS- and LPS-stimulated BMDMs based on TE analysis.

(G) Representative images showing puromycin (green) incorporation in KS- (24 h) and LPS- (6 h) stimulated BMDMs; nuclei were stained with DAPI (blue). Scale bars, 20 μm.

(H) Quantification of puromycin intensity, representing translation rates. Fluorescence intensity was measured from 8 representative images across three independent experiments. Data are presented as mean ± SEM; ****$p < 0.0001$, unpaired *t* test.

(I) GSEA of TE in KS-stimulated BMDMs from RiboTag-seq by GO term "Translation". TE was quantitated by the ratio of RiboTagged transcripts versus bulk mRNA signals.

(J) Read densities of RiboTagged transcripts (upper) and mRNA (lower) of EIF4B in KS-stimulated and control BMDMs from RiboTag-seq. Dashed squares represent the coding region.

approach utilized Cre-mediated deletion to induce the expression of an hemagglutinin epitope-tagged ribosomal subunit in murine macrophages, enabling immunoprecipitation of tagged ribosomes along with associated mRNAs (RiboTagged transcripts) (Figure 2C). To distinguish transcriptional versus translational regulation under CRS condition, we categorized protein-coding genes into four classes based on mRNA and RiboTagged transcript levels (Figure 2D). Notably, the largest cluster was Class I, characterized by genes exhibiting increased translation without corresponding transcriptional upregulation

Please cite this article in press as: Liu et al., Discovery, delineation, and therapeutic targeting of a hyper-translation pathway driving cytokine release syndrome, Cell Reports Medicine (2025), https://doi.org/10.1016/j.xcrm.2025.102531

(Figure 2E), underscoring hyper-translation as a dominant feature of CRS. Indeed, 25% of protein-coding genes in macrophages displayed translation upregulation in the CRS condition, compared to 6.5% in LPS-stimulated cells (Figure 2F). In contrast, transcriptome alterations were comparable between KS and LPS conditions and thus could not account for the CRS-specific effects (Figures S2B and S2C). Translatome analyses were further corroborated by puromycin incorporation assays, showing robust puromycin signals in KS but not in LPS-treated macrophages (Figures 2G and 2H). Among the Class I genes, translation-related genes were highly enriched (Figure 2I), including components of the translation machinery such as EIF4B, which exhibited enhanced RiboTagged transcript signals despite unchanged mRNA levels (Figure 2J). Protein levels of several Class I genes were further verified (Figure S2D). In conclusion, these results systematically validate MHT as a hallmark of CRS, driven by translational rather than transcriptional reprogramming.

CRISPR screening in primary macrophages identifies key mediators of CRS

Next, we wished to delineate the factors and pathways linking MHT with inflammatory output in CRS. Given the limited knowledge of translational regulation in this context,[19] we undertook a systematic approach using a CRISPR-based genetic screen. To ensure the screening efficiency, it was necessary to select a robust readout, which was ideally both highly inducible and exhibited translational enhancement in CRS. Among common cytokine and chemokine coding genes highly expressed by macrophages, RiboTag-seq analysis identified *Il6* as having the highest TE (Figure 3A). Further quantification of the ''translation index'', which compares newly synthesized protein to real-time mRNA levels, demonstrated that KS stimulation induced sustained IL-6 production (Figures S3A and S3B) and heightened translational activity relative to LPS stimulation (Figure 3B). To validate the contribution of translational activation while controlling for *Il6* mRNA variability, we stably expressed exogenous *Il6* transcripts in *Il6*-deficient macrophages. Despite unaltered *Il6* mRNA levels (Figure S3C), translational activity was markedly upregulated under CRS conditions, as indicated by the translation index (Figures 3C and S3D). In general, multiple quantitative approaches support the notion that IL-6 undergoes hyper-translation in CRS, making it a suitable readout of subsequent screening.

Subsequently, we performed a CRISPR screen in Cas9-expressing murine primary macrophages with a macrophage-specific library using IL-6 as the readout (Figure 3D). The screening results enriched multiple candidate genes under CRS condition (Figure 3E) and revealed four functional gene clusters (Figure 3F): signaling components, RNA-binding proteins, transcription factors, and vesicle transport machinery. Protein interaction networks highlighted signaling pathways as central regulators, with the signaling adaptor gene *Pik3ap1* at the initiating node (Figure 3G). Validation using two different single guide RNAs (sgRNAs) showed *Pik3ap1* knockdown reduced KS-induced IL-6 production (Figure S3E), suggesting that *Pik3ap1* is a key positive regulator of IL-6 in the CRS condition.

BCAP mediates macrophage hyper-translation

B-cell adaptor for PI3K (BCAP, protein name for *Pik3ap1*), originally identified as a regulator of B cell development,[27,28] exhibits multifaceted roles across immune cells,[29–34] but its role in CRS is still elusive. We generated myeloid-specific BCAP knockout mice, which exhibited normal myeloid cell development in multiple tissues (Figures 4A and S4A–S4D). Then we explored the function of BCAP in the CRS condition. BCAP deletion did not affect *Il6* mRNA levels in macrophages but significantly reduced IL-6 protein production upon KS stimulation (Figures 4B and 4C), accompanied by diminished newly synthesized IL-6 and a lower IL-6 translation index (Figures 4D and 4E), establishing BCAP as a translational regulator of IL-6 production.

Moreover, BCAP-deficient macrophages exhibited impaired translation activation, as evidenced by reduced puromycin incorporation and decreased ribosome-mRNA association (Figures 4F–4H). Integrated Ribo-seq and RNA sequencing (RNA-seq) revealed that BCAP deletion led to a significant reduction in translation activity, with minimal changes in the transcriptome (Figures 4I and 4J). Specifically, translation-related genes were significantly downregulated at both the RPF and TE levels in the absence of BCAP, while mRNA levels remained largely unchanged (Figures 4K–4M). This was corroborated by reduced levels of translation machinery proteins and other cellular components in BCAP-deficient macrophages (Figures 4N and S4E). In summary, our findings establish BCAP as a crucial mediator of MHT in CRS.

RSK is the downstream pivot for CRS-induced macrophage hyper-translation

Given that BCAP acts as an upstream signaling adaptor, we investigated the mechanistic link between BCAP and hyper-translation. BCAP deficiency selectively impaired phosphatidylinositol 3-kinase (PI3K)-AKT signaling (Figure S5A), with minimal impact on mammalian target of rapamycin (mTOR) activation (Figure S5B). Rapamycin treatment further confirmed the dispensability of mTOR in CRS-associated IL-6 overproduction (Figure S5C), redirecting our investigation to alternative translation regulators. Notably, BCAP-deficient macrophages exhibited markedly reduced phosphorylation and activation of p90 ribosomal S6 kinase (RSK) upon KS stimulation (Figure 5A), suggesting RSK as a potential mediator of MHT. RSK phosphorylates multiple substrates, including EIF4B, a translation initiation factor.[16,35] Concomitant with reduced RSK activity, EIF4B phosphorylation was also diminished in BCAP-deficient cells (Figure 5A). Moreover, RSK phosphorylation and activation were dependent on PI3K and 3′-phosphoinositide-dependent kinase-1 (PDK1) (Figures S5D and S5E). Taken together, these findings implicate the RSK-EIF4B axis as a downstream effector pathway of BCAP.

To genetically assess the role of RSK in CRS, we generated RSK1 (gene name *Rps6ka1*) knockout mice (Figure 5B), as RSK1 is the predominant isoform in macrophages (Figure S5F). These mice exhibited normal growth and immune cell development (Figures S5G–S5K). However, RSK1 deletion led to reduced IL-6 translation upon KS stimulation, without affecting *Il6* mRNA levels (Figures 5C–5F). Similar to the BCAP knockout phenotypes, RSK1-deficient macrophages displayed impaired

Please cite this article in press as: Liu et al., Discovery, delineation, and therapeutic targeting of a hyper-translation pathway driving cytokine release syndrome, Cell Reports Medicine (2025), https://doi.org/10.1016/j.xcrm.2025.102531

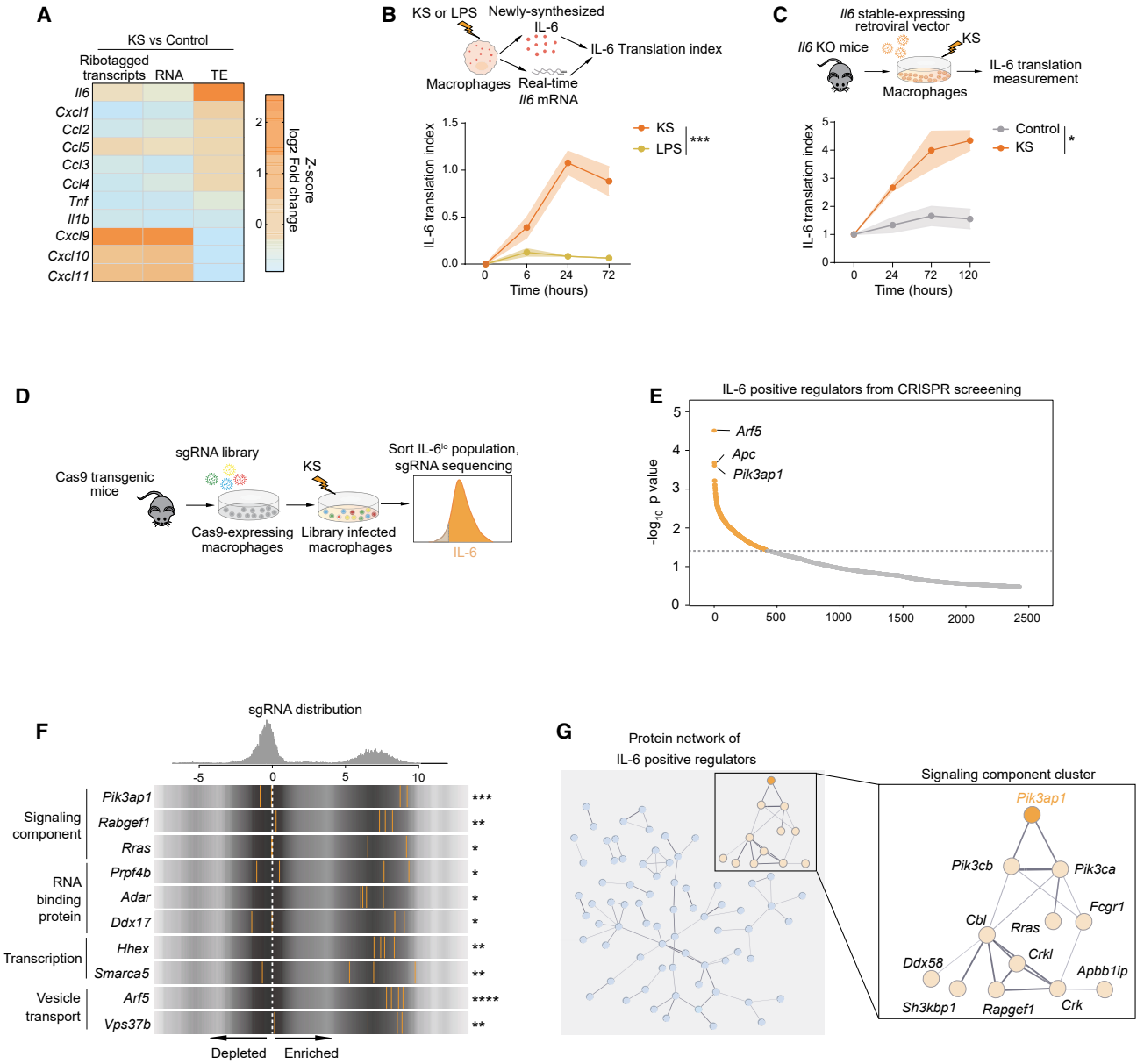

Figure 3. CRISPR screening in primary macrophages identifies key mediators of CRS

(A) Heatmap of RiboTagged transcripts, RNA, and TE of cytokine- and chemokine-coding genes in KS-stimulated BMDMs from RiboTag-seq.

(B) Schematic of IL-6 translation index by measurement of newly synthesized IL-6 and real-time *Il6* mRNA levels (upper). IL-6 translation index was measured in KS- and LPS-stimulated BMDMs normalized to 24 h KS group (lower, $n = 4$).

(C) Schematic of IL-6 translation measurement in *Il6*-overexpression system (upper) and corresponding IL-6 translation index after KS stimulation normalized to 0 h (lower, $n = 3$). Data in (B and C) are presented as mean ± SEM; p values were calculated by two-way ANOVA. $^{*}p < 0.05$, $^{***}p < 0.001$.

(D) Schematic of CRISPR screen workflow in BMDMs.

(E) Scatterplot of candidate genes from CRISPR screen. Genes with p value <0.05 were in orange, and top three genes were labeled.

(F) sgRNA distribution plot from CRISPR screen. Four sgRNAs per gene are in orange. p values were calculated by MaGeCK tool. $^{*}p < 0.05$, $^{**}p < 0.01$, $^{***}p < 0.001$, $^{****}p < 0.0001$.

(G) Protein-protein interaction network of candidate genes with p value <0.05. Signaling component genes are in orange, and top hit gene *Pik3ap1* was highlighted.

translation activation, as evidenced by decreased puromycin incorporation and ribosome-mRNA association (Figures 5G–5I). RNA-seq analysis demonstrated that RSK1 had minimal impact on macrophage transcriptome (Figure 5J), indicating that RSK1 primarily influenced translation rather than transcription. Correspondingly, EIF4B activation and the protein levels of translation machinery components were reduced in RSK1-deficient cells (Figure 5K, 5L, and S5L). Inhibition of EIF4A/EIF4B

Please cite this article in press as: Liu et al., Discovery, delineation, and therapeutic targeting of a hyper-translation pathway driving cytokine release syndrome, Cell Reports Medicine (2025), https://doi.org/10.1016/j.xcrm.2025.102531

CellPress
OPEN ACCESS

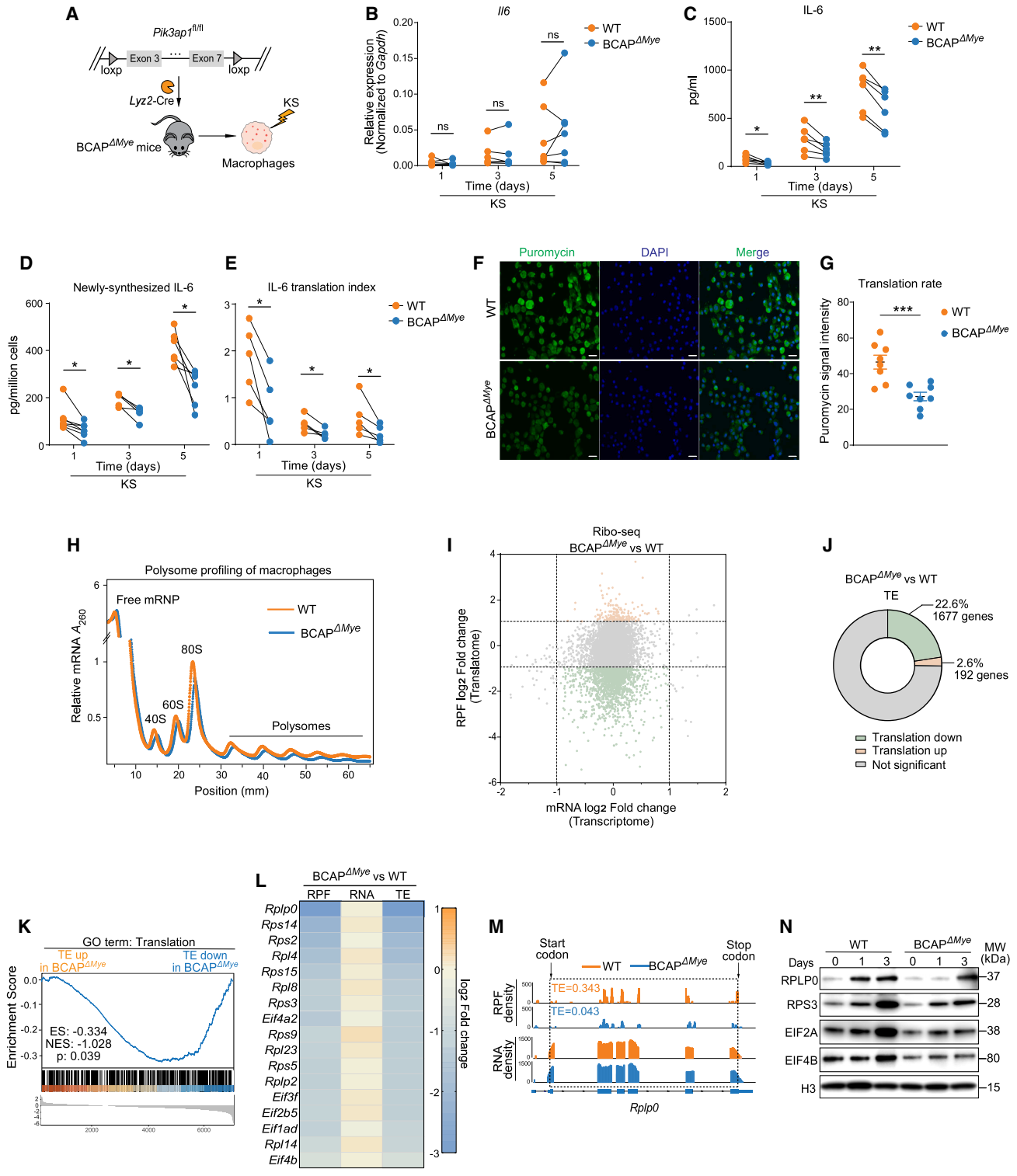

Figure 4. BCAP is responsible for macrophage hyper-translation in CRS

(A) Schematic of generation of myeloid-specific BCAP knockout mice and subsequent BMDM stimulation.

(B and C) IL-6 mRNA levels and protein production of BCAP-deficient BMDMs after KS stimulation, respectively (n = 6).

(D and E) Newly synthesized IL-6 and IL-6 translation index in BCAP-deficient BMDMs after KS stimulation, respectively (n = 5).

(legend continued on next page)

Please cite this article in press as: Liu et al., Discovery, delineation, and therapeutic targeting of a hyper-translation pathway driving cytokine release syndrome, Cell Reports Medicine (2025), https://doi.org/10.1016/j.xcrm.2025.102531

activity significantly attenuated IL-6 translation, establishing the RSK-EIF4B axis as a direct regulator of both IL-6 synthesis and hyper-translation (Figure S5M). Furthermore, chemical inhibition of RSK using a small molecule inhibitor LJH685 effectively dampened IL-6 production at the translational level without inhibiting *Il6* mRNA (Figures 5M–5P). Moreover, LJH685 suppressed global protein synthesis in CRS (Figures S5N and S5O). Neither RSK1 ablation nor pharmacological RSK inhibition impaired TLR ligand-induced IL-6 production (Figures S5P and S5Q), establishing a selective requirement for RSK in promoting CRS-associated inflammation. Collectively, these findings establish RSK as a crucial downstream mediator of CRS-induced MHT.

Targeting translation via RSK inhibition ameliorates CRS

Building on the above findings that highlight the role of MHT in CRS pathogenesis, we explored the therapeutic potential of targeting translation. To enhance the disease relevance, we validated the function of RSK in human primary monocytes. Consistent with the murine loss-of-function phenotypes, silencing RSK1 in human monocytes upon KS stimulation resulted in reduced IL-6 production without affecting mRNA levels (Figures 6A and S6A). Additionally, RSK inhibition using the compound LJH685 effectively decreased IL-6 production at the translation level without compromising the viability of human monocytes (Figures 6B, S6B, and S6C). These results suggest that RSK inhibition could be a promising therapeutic strategy for CRS.

To evaluate the therapeutic potential of RSK inhibition in a clinically relevant context, we assessed its effects in a humanized CRS mouse model, where human cord blood-derived hematopoietic stem cells were transplanted into immune-compromised mice, followed by injection of tumor cells and human syngeneic CAR T cells (Figure 6C). Treatment with LJH685 in humanized mice significantly alleviated fever and CRS-associated weight loss (Figures 6D and 6E). Moreover, serum IL-6 levels were markedly decreased in LJH685-treated mice (Figure 6F), with no significant changes in mRNA levels (Figure S6D). Crucially, LJH685 treatment did not impair CAR T cell-mediated tumoricidal activity or CAR T cell expansion (Figures 6G and 6H). Histological analysis of multiple organs revealed no signs of graft-versus-host disease following CAR T cell infusion, and LJH685 did not cause visible organ toxicity (Figure S6E). These data indicate that targeting translation through RSK inhibition effectively ameliorates CRS in a humanized model. Collectively, the above findings support the notion that monocyte/macrophage hyper-translation is a previously unrecognized hallmark that distinguishes CRS from resolvable inflammation and can be therapeutically targeted (Figure 6I).

DISCUSSION

To characterize the immune abnormalities underlying CRS, we began by analyzing patient samples during disease progression and identified widespread boost of protein translation including, but not limited to, upregulation of inflammatory mediators, which we define as MHT. We then employed an unbiased CRISPR screening approach to dissect the molecular pathways driving MHT, which revealed the BCAP-RSK signaling axis as a critical regulator. Notably, RSK, being a kinase, presented a druggable target; pharmacological inhibition of RSK mitigated CRS severity in a humanized mouse model without compromising CAR T antitumor efficacy. This bedside-to-bench investigative pipeline not only established hyper-translation as a hallmark of dysregulated inflammatory responses in CRS but also discovered and therapeutically validated a targetable pathway driving pathological inflammation in this condition (Figure S6F).

Protein synthesis is an energy-intensive process that must be tightly regulated under normal physiological conditions. However, excessive translation is observed in certain pathological states, such as cancer, where pro-translation oncogenic signaling pathways and mutations in core translational machinery drive uncontrolled growth of tumor cells.[36] Intriguingly, monocytes and macrophages also ramp up translation during CRS, potentially as an emergent stress-adaptive mechanism. A key pathway driving this hyper-translation is the BCAP-RSK cascade. While BCAP was originally identified in B cells, its homology with the Dof protein in *Drosophila*,[27] which lacks B cells, suggests a broader role in innate immunity. In fact, BCAP has been described as a negative regulator of TLR signaling in myeloid cells, damping inflammatory gene transcription.[30,31] Paradoxically, in the context of CRS, BCAP shifts to a pro-inflammatory role by enhancing the translation of inflammatory mediators such as IL-6. This dual function raises a compelling therapeutic possibility: targeting the BCAP-RSK axis might selectively suppress pathological hyperinflammation in CRS while preserving beneficial inflammatory responses essential for host defense, such as those triggered by TLR ligands.

Indeed, genetic ablation or pharmacological inhibition of RSK did not suppress TLR-induced inflammation, indicating that RSK is a selective driver of pathological hyperinflammation rather than a universal mediator of inflammatory responses. The therapeutic viability of targeting RSK is further underscored by its ongoing exploration in oncology: the RSK inhibitor PMD-026 is currently in phase 2 trials for metastatic breast cancer (NCT04115306),[37] demonstrating its clinical safety profile. Targeting RSK in the context of immune responses presents a therapeutic strategy for inflammatory diseases. Supporting the safety of this approach,

(F and G) Representative images showing puromycin (green) incorporation in KS-stimulated (24 h) wild-type (WT) and BCAP-deficient BMDMs; nuclei were stained with DAPI (blue). Scale bars, 20μm. Translation rate quantitated by puromycin intensity is shown in (G). Quantification of puromycin intensity, representing translation rates. Fluorescence intensity was measured from 8 representative images across three independent experiments.
(H) Polysome profiling of BCAP-deficient versus WT BMDMs after KS stimulation (24 h). A_{260} absorbance was normalized to the 80S peak value of WT group.
(I) Scatterplot of translatome and transcriptome of BCAP-deficient versus WT BMDM after KS stimulation (24 h) from Ribo-seq.
(J) Schematic of translatome alteration in BCAP-deficient BMDMs by TE analysis.
(K) GSEA of TE in KS-stimulated BCAP-deficient BMDMs by GO term "Translation".
(L) Heatmap of core translation machinery genes RPF, RNA, and TE in BCAP-deficient BMDMs after KS stimulation.
(M) Read densities of RPF (upper) and mRNA (lower) of *Rplp0* in WT and BCAP-deficient BMDMs from Ribo-seq. Dashed squares represent the coding region.
(N) Western blot analysis of translation machinery in WT and BCAP-deficient BMDMs. Representative data of three independent experiments. Data in (G) are presented as mean ± SEM; $^{*}p < 0.05$, $^{**}p < 0.01$, $^{***}p < 0.001$, ns, not significant, paired *t* test in (B–E) and unpaired *t* test in (H).

Please cite this article in press as: Liu et al., Discovery, delineation, and therapeutic targeting of a hyper-translation pathway driving cytokine release syndrome, Cell Reports Medicine (2025), https://doi.org/10.1016/j.xcrm.2025.102531

CellPress
OPEN ACCESS

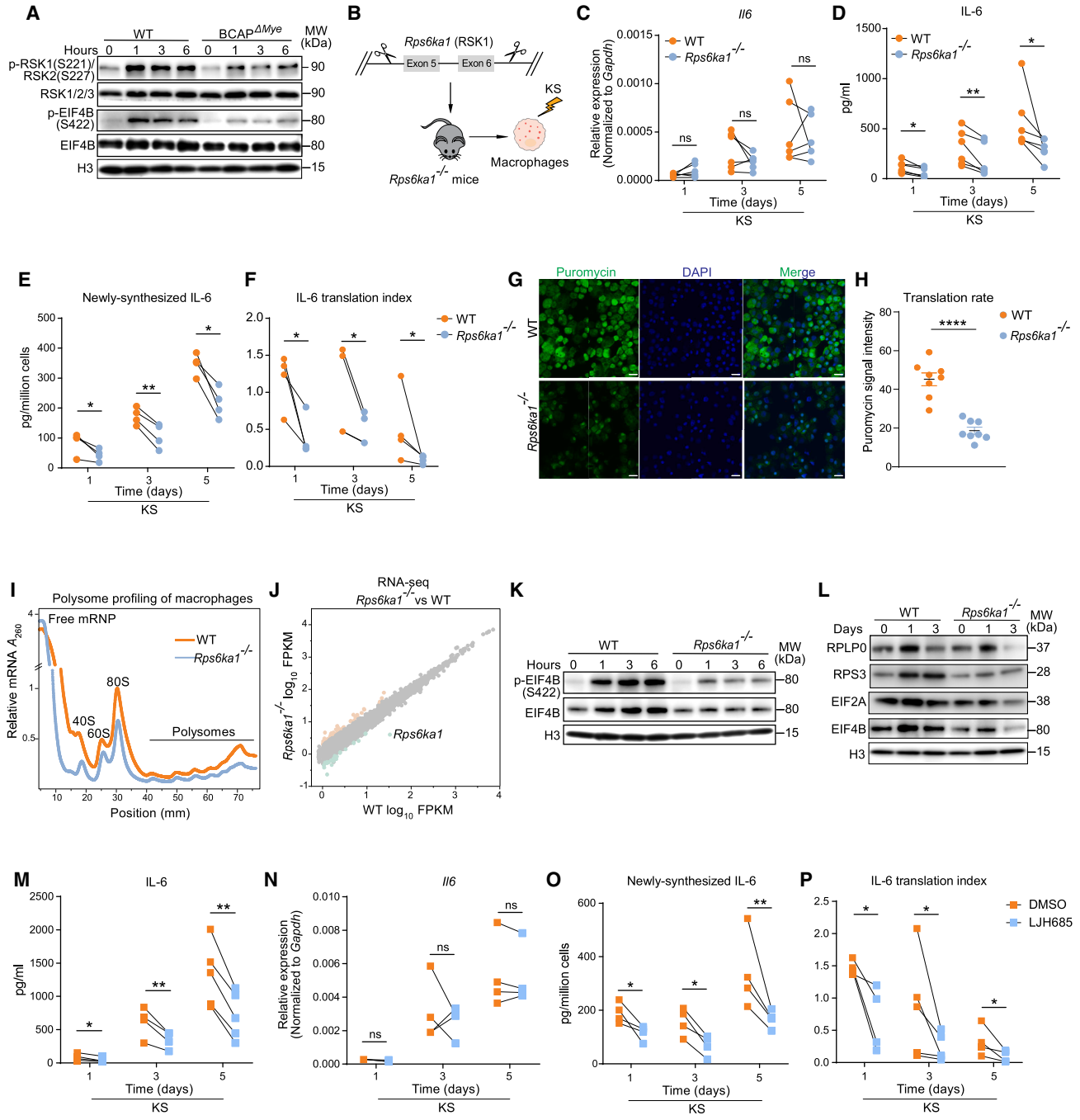

Figure 5. RSK is the downstream signaling pivot of BCAP and promotes macrophage hyper-translation in CRS

(A) Western blot analysis of RSK-EIF4B activation in BCAP-deficient BMDMs. Representative data of three independent experiments.

(B) Schematic of the generation of RSK1 knockout mice and subsequent BMDM stimulation.

(C and D) IL-6 mRNA levels and protein production in RSK1-deficient BMDMs after KS stimulation, respectively (n = 6).

(E and F) Newly synthesized IL-6 and IL-6 translation index of RSK1-deficient BMDMs after KS stimulation, respectively (n = 4).

(G and H) Representative images showing puromycin (green) incorporation in KS-stimulated (24 h) WT and RSK1-deficient BMDMs; nuclei were stained with DAPI (blue). Scale bars, 20 μm. Translation rate quantitated by puromycin intensity is shown in (H). Quantification of puromycin intensity, representing translation rates. Fluorescence intensity was measured from 8 representative images across three independent experiments.

(I) Polysome profiling of RSK1-deficient versus WT BMDMs after KS stimulation (24 h). A_{260} absorbance was normalized to 80S peak value of WT group.

(J) Scatterplot of transcriptome of RSK1-deficient versus WT BMDMs after KS stimulation (24 h) from RNA-seq. *Rps6ka1* was marked as indicated.

(legend continued on next page)

Please cite this article in press as: Liu et al., Discovery, delineation, and therapeutic targeting of a hyper-translation pathway driving cytokine release syndrome, Cell Reports Medicine (2025), https://doi.org/10.1016/j.xcrm.2025.102531

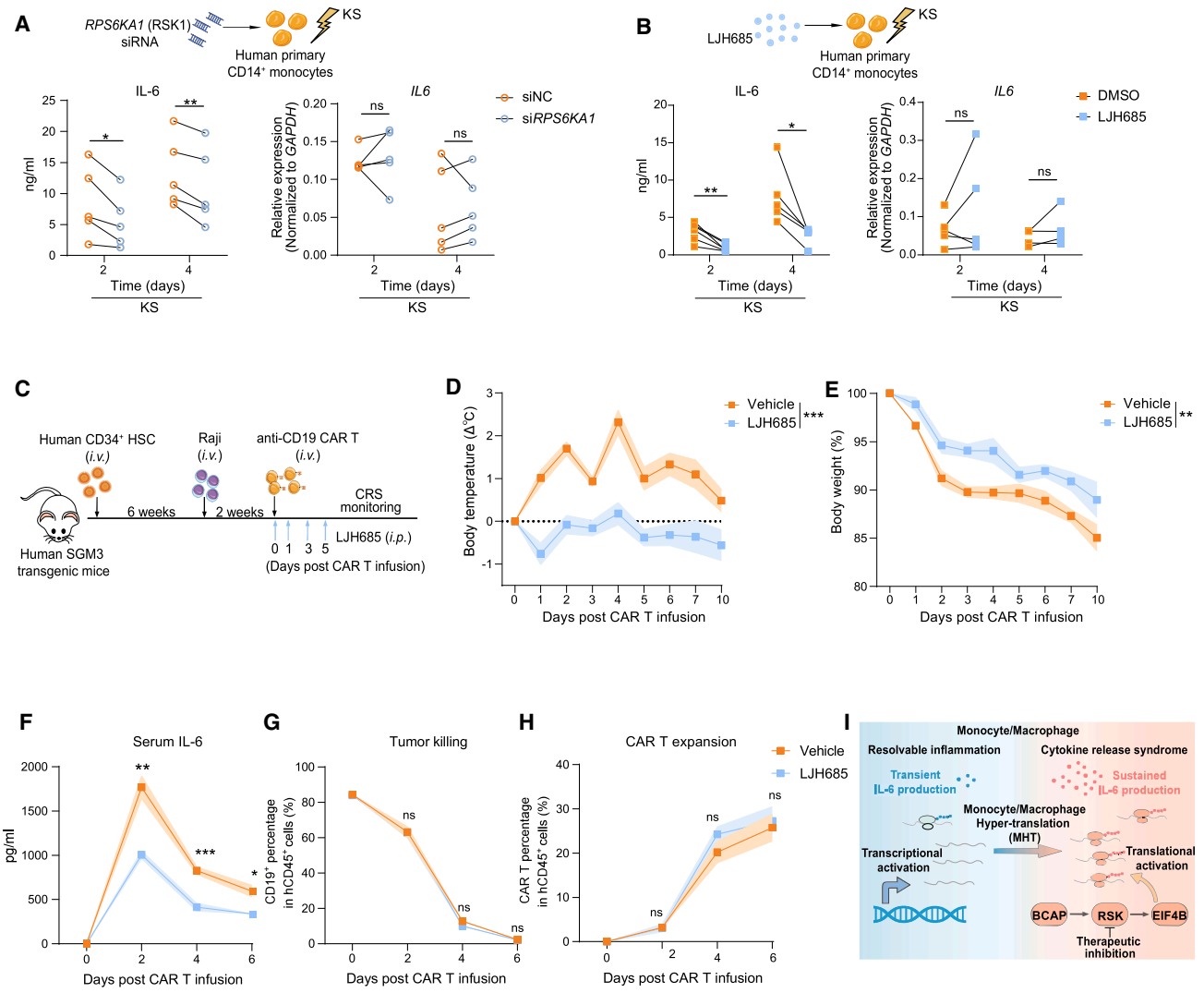

Figure 6. RSK inhibition ameliorated CRS in humanized models

(A) Schematic of siRNA-mediated *RPS6KA1* (RSK1) knockdown in human primary CD14$^+$ monocytes (upper). IL-6 production (lower left) and *IL6* mRNA levels (lower right) in *RPS6KA1*-knockdown monocytes.

(B) Schematic of RSK inhibitor LJH685 treatment (1μM, upper) and IL-6 production (lower left) along with *IL6* mRNA levels (lower right) in LJH685-treated monocytes.

(C) Schematic of humanized mouse model and CRS induction. Arrows indicate timing of 20 mg/kg LJH685 administration.

(D–H) Body temperature, body weight, serum IL-6 levels, tumor killing, and CAR T cell expansion in LJH685-treated humanized CRS mice ($n = 5$). Data in (D–H) are presented as mean ± SEM; $^*p < 0.05$, $^{**}p < 0.01$, $^{***}p < 0.001$, ns, not significant, paired *t* test in (A and B), unpaired *t* test in (F–H) and two-way ANOVA in (D and E).

(I) Schematic of molecular mechanism underlying MHT in CRS. In resolvable inflammation, transcription activation mechanism dictates the transient IL-6 production. In CRS, uncontrolled inflammation depends on the hyper-translation pathway and triggered sustained IL-6 production.

RSK1 knockout mice exhibit normal development, and combined deletion of RSK1/2/3 does not compromise viability or fertility.[38] Moreover, in our humanized CRS mouse model, administration of RSK inhibitors did not elicit notable adverse effects (Figure S6E and data not shown), further validating the safety of targeting this translational pathway. Collectively, our data propose RSK as a promising therapeutic target for CRS, paving the way for translation-oriented drug discovery in inflammatory diseases.

Increasing evidence suggests that modulation of translation machinery has the potential to profoundly impact inflammatory

(K) EIF4B activation in RSK1-deficient BMDMs after KS stimulation. Representative data of three independent experiments.

(L) Western blot analysis of translation machinery in WT and RSK1-deficient BMDMs. Representative data of three independent experiments.

(M–P) IL-6 protein levels, mRNA levels, newly synthesized IL-6, and IL-6 translation index of RSK inhibitor LJH685 (1μM)-treated BMDMs, respectively. Data in (H) are presented as mean ± SEM; $^*p < 0.05$, $^{**}p < 0.01$, $^{****}p < 0.0001$, ns, not significant, paired *t* test in (C–F and M–P) and unpaired *t* test in (H).

responses.[18,21] For instance, enhanced translation of interferon regulatory factor (IRF) 8 (IRF8) promotes macrophage inflammatory polarization.[39] One key mechanism through which interferon-γ primes macrophage activation involves the suppression of EIF4E, which otherwise facilitates the translation of negative regulators of inflammation.[40] Additionally, mTOR-4E-binding protein pathway regulates the translation of immune mediators,[41–45] such as IRF7, thereby influencing interferon production and antiviral responses.[41] Beyond translation initiation, elongation also serves as a critical regulatory node in inflammatory responses. The eukaryotic elongation factor 2 kinase (EEF2K)-eukaryotic elongation factor 2 (EEF2) axis, for example, regulates the translation of proinflammatory cytokines in pathological settings.[22,46] Previously, we demonstrated that metoprolol alleviates CRS in patients by targeting IL-6 translation. In this study, we uncover a pathway of translational control that operates independently of metoprolol's effect in CRS. Mechanistically, metoprolol attenuates EEF2K-EEF2-mediated translation elongation,[22] acting as a brake on IL-6 protein synthesis. In contrast, the BCAP-RSK axis promotes translation initiation, serving as an upstream driver of MHT. Notably, metoprolol had no significant impact on the translation initiation machinery, and BCAP deficiency did not diminish EEF2 activity (data not shown). These observations suggest that translation is regulated through sequential and multifaceted mechanisms, mirroring the layered complexity of transcriptional control. While this work provides initial insights, further research is needed to fully unravel the intricate networks of translational regulation and harness their therapeutic potential for treating human inflammatory diseases.

Limitations of the study

A limitation of our study is that the CRS models and patient samples we analyzed were limited to CAR T therapy-induced CRS. CRSs are heterogeneous and can arise from diverse triggers. For example, severe infectious pathogens can produce CRS-like manifestations. We did not examine infection-associated or other non-CAR T causes of CRS, so it remains uncertain whether hyper-translation occurs in those contexts or whether it similarly drives inflammatory responses.

Although our study identified hyper-translation as a hallmark and potential therapeutic target of CRS, the precise factors initiating this response remain undetermined. The stimuli driving hyper-translation could originate from CAR T cells, lysed tumor cells, activated macrophages, or soluble mediators released during target cell killing, but the relative importance of these components remains to be clarified. Moreover, while we demonstrated the feasibility of targeting RSK as a therapeutic strategy in animal models, human CRS represents a highly heterogeneous condition with complex clinical manifestations. Thus, the translational relevance of RSK inhibition to human CRS and other inflammatory diseases remains to be established, including whether suitable small-molecule inhibitors can achieve safety and efficacy in clinical settings.

RESOURCE AVAILABILITY

Lead contact

Further information and requests for resources and reagents should be directed to and will be fulfilled by the lead contact, Xiaoyu Hu (huxiaoyu@westlake.edu.cn).

Materials availability

This study did not generate new unique reagents. Plasmids generated in this study are available upon request.

Data and code availability

- New data generated in this study were deposited in Gene Expression Omnibus database under accession Ribo-seq (GSE287440, GSE287441, and GSE287444), RiboTag-seq (GSE287442), CRISPR screen (GSE287443), and RNA-seq (GSE287445).
- This paper does not report original code.
- Any additional information required to reanalyze the data reported in this paper is available from the lead contact upon request.

ACKNOWLEDGMENTS

We thank the patients and their families for their contribution to scientific research. We thank the core facility at the Institute for Immunology, Tsinghua University, for valuable technical assistance. We thank members of the Hu laboratory for discussion and technical consultation. We thank Dr. Wenwen Zeng, Dr. Huabing Li, and Dr. Min Peng for providing valuable research tools. This work was supported by National Key Research and Development Program of China (2023YFC2306200 and 2020YFA0509100 to X.H.), National Natural Science Foundation of China (32030037 and 32430034 to X.H., 82341208 and 82430012 to W.H., and 32070951 to Y.Z.), National Science and Technology Major Project of China (2023ZD0501303 to W.H.), funds from Tsinghua-Peking Center for Life Sciences (X.H.), and the R&D Program of Guangzhou National Laboratory grant GZNL2023A01009 (to X.H.).

AUTHOR CONTRIBUTIONS

X. Liu and J.L. designed and performed experiments, analyzed and interpreted data, and wrote the manuscript. Y.Z., Yang Liu, C.W., and Y.W. collected human samples and performed experiments. Yunqi Liu and Y.Y. performed experiments and analyzed data. Y.S. analyzed ribosome profiling and RNA-seq datasets. Y. Lu, W.W., Y.-X.F., X. Lin, and D.P. provided key reagents and advice. X.H. and W.H. conceptualized the project, supervised experiments, interpreted data, and wrote the manuscript.

DECLARATION OF INTERESTS

The authors declare no competing interests.

STAR★METHODS

Detailed methods are provided in the online version of this paper and include the following:

SUPPLEMENTAL INFORMATION

Supplemental information can be found online at https://doi.org/10.1016/j.xcrm.2025.102531.

Received: April 23, 2025
Revised: August 17, 2025
Accepted: November 21, 2025

REFERENCES

1. Medzhitov, R. (2008). Origin and physiological roles of inflammation. Nature *454*, 428–435. https://doi.org/10.1038/nature07201.
2. Hotamisligil, G.S. (2017). Inflammation, metaflammation and immunometabolic disorders. Nature *542*, 177–185. https://doi.org/10.1038/nature21363.
3. Meizlish, M.L., Franklin, R.A., Zhou, X., and Medzhitov, R. (2021). Tissue Homeostasis and Inflammation. Annu. Rev. Immunol. *39*, 557–581. https://doi.org/10.1146/annurev-immunol-061020-053734.
4. Nathan, C. (2002). Points of control in inflammation. Nature *420*, 846–852. https://doi.org/10.1038/nature01320.
5. Gilroy, D.W. (2021). Resolving inflammation. Nat. Rev. Immunol. *21*, 620–621. https://doi.org/10.1038/s41577-021-00597-w.
6. Rothlin, C.V., Carrera-Silva, E.A., Bosurgi, L., and Ghosh, S. (2015). TAM receptor signaling in immune homeostasis. Annu. Rev. Immunol. *33*, 355–391. https://doi.org/10.1146/annurev-immunol-032414-112103.
7. Nathan, C., and Ding, A. (2010). Nonresolving inflammation. Cell *140*, 871–882. https://doi.org/10.1016/j.cell.2010.02.029.
8. Fajgenbaum, D.C., and June, C.H. (2020). Cytokine Storm. N. Engl. J. Med. *383*, 2255–2273. https://doi.org/10.1056/NEJMra2026131.
9. Morris, E.C., Neelapu, S.S., Giavridis, T., and Sadelain, M. (2022). Cytokine release syndrome and associated neurotoxicity in cancer immunotherapy. Nat. Rev. Immunol. *22*, 85–96. https://doi.org/10.1038/s41577-021-00547-6.
10. Brudno, J.N., and Kochenderfer, J.N. (2024). Current understanding and management of CAR T cell-associated toxicities. Nat. Rev. Clin. Oncol. *21*, 501–521. https://doi.org/10.1038/s41571-024-00903-0.
11. Giavridis, T., van der Stegen, S.J.C., Eyquem, J., Hamieh, M., Piersigilli, A., and Sadelain, M. (2018). CAR T cell-induced cytokine release syndrome is mediated by macrophages and abated by IL-1 blockade. Nat. Med. *24*, 731–738. https://doi.org/10.1038/s41591-018-0041-7.
12. Norelli, M., Camisa, B., Barbiera, G., Falcone, L., Purevdorj, A., Genua, M., Sanvito, F., Ponzoni, M., Doglioni, C., Cristofori, P., et al. (2018). Monocyte-derived IL-1 and IL-6 are differentially required for cytokine-release syndrome and neurotoxicity due to CAR T cells. Nat. Med. *24*, 739–748. https://doi.org/10.1038/s41591-018-0036-4.
13. Xing, X., and Hu, X. (2023). Risk factors of cytokine release syndrome: stress, catecholamines, and beyond. Trends Immunol. *44*, 93–100. https://doi.org/10.1016/j.it.2022.12.003.
14. Medzhitov, R., and Horng, T. (2009). Transcriptional control of the inflammatory response. Nat. Rev. Immunol. *9*, 692–703. https://doi.org/10.1038/nri2634.
15. Kawai, T., and Akira, S. (2010). The role of pattern-recognition receptors in innate immunity: update on Toll-like receptors. Nat. Immunol. *11*, 373–384. https://doi.org/10.1038/ni.1863.
16. Brito Querido, J., Díaz-López, I., and Ramakrishnan, V. (2024). The molecular basis of translation initiation and its regulation in eukaryotes. Nat. Rev. Mol. Cell Biol. *25*, 168–186. https://doi.org/10.1038/s41580-023-00624-9.
17. Parker, R., and Sheth, U. (2007). P bodies and the control of mRNA translation and degradation. Mol. Cell *25*, 635–646. https://doi.org/10.1016/j.molcel.2007.02.011.
18. Piccirillo, C.A., Bjur, E., Topisirovic, I., Sonenberg, N., and Larsson, O. (2014). Translational control of immune responses: from transcripts to translatomes. Nat. Immunol. *15*, 503–511. https://doi.org/10.1038/ni.2891.
19. Liu, X., Han, W., and Hu, X. (2023). Post-transcriptional regulation of myeloid cell-mediated inflammatory responses. Adv. Immunol. *160*, 59–82. https://doi.org/10.1016/bs.ai.2023.09.001.
20. Lindqvist, L.M., Tandoc, K., Topisirovic, I., and Furic, L. (2018). Cross-talk between protein synthesis, energy metabolism and autophagy in cancer. Curr. Opin. Genet. Dev. *48*, 104–111. https://doi.org/10.1016/j.gde.2017.11.003.
21. Carpenter, S., Ricci, E.P., Mercier, B.C., Moore, M.J., and Fitzgerald, K.A. (2014). Post-transcriptional regulation of gene expression in innate immunity. Nat. Rev. Immunol. *14*, 361–376. https://doi.org/10.1038/nri3682.
22. Yang, Y., Zhang, Y., Xing, X., Xu, G., Lin, X., Wang, Y., Chen, M., Wang, C., Zhang, B., Han, W., and Hu, X. (2023). IL-6 translation is a therapeutic target of human cytokine release syndrome. J. Exp. Med. *220*, e20230577. https://doi.org/10.1084/jem.20230577.
23. Schmidt, E.K., Clavarino, G., Ceppi, M., and Pierre, P. (2009). SUnSET, a nonradioactive method to monitor protein synthesis. Nat. Methods *6*, 275–277. https://doi.org/10.1038/nmeth.1314.
24. Ingolia, N.T., Brar, G.A., Rouskin, S., McGeachy, A.M., and Weissman, J.S. (2012). The ribosome profiling strategy for monitoring translation in vivo by deep sequencing of ribosome-protected mRNA fragments. Nat. Protoc. *7*, 1534–1550. https://doi.org/10.1038/nprot.2012.086.
25. Ingolia, N.T., Ghaemmaghami, S., Newman, J.R.S., and Weissman, J.S. (2009). Genome-wide analysis in vivo of translation with nucleotide resolution using ribosome profiling. Science *324*, 218–223. https://doi.org/10.1126/science.1168978.
26. Sanz, E., Yang, L., Su, T., Morris, D.R., McKnight, G.S., and Amieux, P.S. (2009). Cell-type-specific isolation of ribosome-associated mRNA from complex tissues. Proc. Natl. Acad. Sci. USA *106*, 13939–13944. https://doi.org/10.1073/pnas.0907143106.
27. Okada, T., Maeda, A., Iwamatsu, A., Gotoh, K., and Kurosaki, T. (2000). BCAP: the tyrosine kinase substrate that connects B cell receptor to phosphoinositide 3-kinase activation. Immunity *13*, 817–827. https://doi.org/10.1016/s1074-7613(00)00079-0.
28. Yamazaki, T., Takeda, K., Gotoh, K., Takeshima, H., Akira, S., and Kurosaki, T. (2002). Essential immunoregulatory role for BCAP in B cell development and function. J. Exp. Med. *195*, 535–545. https://doi.org/10.1084/jem.20011751.
29. MacFarlane, A.W., 4th, Yamazaki, T., Fang, M., Sigal, L.J., Kurosaki, T., and Campbell, K.S. (2008). Enhanced NK-cell development and function in BCAP-deficient mice. Blood *112*, 131–140. https://doi.org/10.1182/blood-2007-08-107847.
30. Ni, M., MacFarlane, A.W., 4th, Toft, M., Lowell, C.A., Campbell, K.S., and Hamerman, J.A. (2012). B-cell adaptor for PI3K (BCAP) negatively regulates Toll-like receptor signaling through activation of PI3K. Proc. Natl. Acad. Sci. USA *109*, 267–272. https://doi.org/10.1073/pnas.1111957108.
31. Troutman, T.D., Hu, W., Fulenchek, S., Yamazaki, T., Kurosaki, T., Bazan, J.F., and Pasare, C. (2012). Role for B-cell adapter for PI3K (BCAP) as a signaling adapter linking Toll-like receptors (TLRs) to serine/threonine kinases PI3K/Akt. Proc. Natl. Acad. Sci. USA *109*, 273–278. https://doi.org/10.1073/pnas.1118579109.
32. Singh, M.D., Ni, M., Sullivan, J.M., Hamerman, J.A., and Campbell, D.J. (2018). B cell adaptor for PI3-kinase (BCAP) modulates CD8(+) effector and memory T cell differentiation. J. Exp. Med. *215*, 2429–2443. https://doi.org/10.1084/jem.20171820.
33. Chu, T., Ni, M., Chen, C., Akilesh, S., and Hamerman, J.A. (2019). Cutting Edge: BCAP Promotes Lupus-like Disease and TLR-Mediated Type I IFN

Induction in Plasmacytoid Dendritic Cells. J. Immunol. *202*, 2529–2534. https://doi.org/10.4049/jimmunol.1801267.

34. Miao, Y., Jiang, M., Qi, L., Yang, D., Xiao, W., and Fang, F. (2020). BCAP Regulates Dendritic Cell Maturation Through the Dual-Regulation of NF-κB and PI3K/AKT Signaling During Infection. Front. Immunol. *11*, 250. https://doi.org/10.3389/fimmu.2020.00250.
35. Anjum, R., and Blenis, J. (2008). The RSK family of kinases: emerging roles in cellular signalling. Nat. Rev. Mol. Cell Biol. *9*, 747–758. https://doi.org/10.1038/nrm2509.
36. Fabbri, L., Chakraborty, A., Robert, C., and Vagner, S. (2021). The plasticity of mRNA translation during cancer progression and therapy resistance. Nat. Rev. Cancer *21*, 558–577. https://doi.org/10.1038/s41568-021-00380-y.
37. Spirrison, A.N., and Lannigan, D.A. (2024). RSK1 and RSK2 as therapeutic targets: an up-to-date snapshot of emerging data. Expert Opin. Ther. Targets *28*, 1047–1059. https://doi.org/10.1080/14728222.2024.2433123.
38. Zaru, R., Matthews, S.P., Edgar, A.J., Prescott, A.R., Gomez-Nicola, D., Hanauer, A., and Watts, C. (2015). The PDK1-Rsk Signaling Pathway Controls Langerhans Cell Proliferation and Patterning. J. Immunol. *195*, 4264–4272. https://doi.org/10.4049/jimmunol.1501520.
39. Xu, H., Zhu, J., Smith, S., Foldi, J., Zhao, B., Chung, A.Y., Outtz, H., Kitajewski, J., Shi, C., Weber, S., et al. (2012). Notch-RBP-J signaling regulates the transcription factor IRF8 to promote inflammatory macrophage polarization. Nat. Immunol. *13*, 642–650. https://doi.org/10.1038/ni.2304.
40. Su, X., Yu, Y., Zhong, Y., Giannopoulou, E.G., Hu, X., Liu, H., Cross, J.R., Rätsch, G., Rice, C.M., and Ivashkiv, L.B. (2015). Interferon-γ regulates cellular metabolism and mRNA translation to potentiate macrophage activation. Nat. Immunol. *16*, 838–849. https://doi.org/10.1038/ni.3205.
41. Colina, R., Costa-Mattioli, M., Dowling, R.J.O., Jaramillo, M., Tai, L.H., Breitbach, C.J., Martineau, Y., Larsson, O., Rong, L., Svitkin, Y.V., et al. (2008). Translational control of the innate immune response through IRF-7. Nature *452*, 323–328. https://doi.org/10.1038/nature06730.
42. Pearl, D., Katsumura, S., Amiri, M., Tabatabaei, N., Zhang, X., Vinette, V., Pang, X., Beug, S.T., Kim, S.H., Jones, L.M., et al. (2020). 4E-BP-Dependent Translational Control of Irf8 Mediates Adipose Tissue Macrophage Inflammatory Response. J. Immunol. *204*, 2392–2400. https://doi.org/10.4049/jimmunol.1900538.
43. William, M., Leroux, L.P., Chaparro, V., Graber, T.E., Alain, T., and Jaramillo, M. (2019). Translational repression of Ccl5 and Cxcl10 by 4E-BP1 and 4E-BP2 restrains the ability of mouse macrophages to induce migration of activated T cells. Eur. J. Immunol. *49*, 1200–1212. https://doi.org/10.1002/eji.201847857.
44. William, M., Leroux, L.P., Chaparro, V., Lorent, J., Graber, T.E., M'Boutchou, M.N., Charpentier, T., Fabié, A., Dozois, C.M., Stäger, S., et al. (2018). eIF4E-Binding Proteins 1 and 2 Limit Macrophage Anti-Inflammatory Responses through Translational Repression of IL-10 and Cyclooxygenase-2. J. Immunol. *200*, 4102–4116. https://doi.org/10.4049/jimmunol.1701670.
45. Jaramillo, M., Gomez, M.A., Larsson, O., Shio, M.T., Topisirovic, I., Contreras, I., Luxenburg, R., Rosenfeld, A., Colina, R., McMaster, R.W., et al. (2011). Leishmania Repression of Host Translation through mTOR Cleavage Is Required for Parasite Survival and Infection. Cell Host Microbe *9*, 331–341. https://doi.org/10.1016/j.chom.2011.03.008.
46. Gonzalez-Teran, B., Cortes, J.R., Manieri, E., Matesanz, N., Verdugo, A., Rodriguez, M.E., Gonzalez-Rodriguez, A., Valverde, A., Martin, P., Davis, R.J., and Sabio, G. (2013). Eukaryotic elongation factor 2 controls TNF-alpha translation in LPS-induced hepatitis. J. Clin. Investig. *123*, 164–178. https://doi.org/10.1172/jci65124.

Please cite this article in press as: Liu et al., Discovery, delineation, and therapeutic targeting of a hyper-translation pathway driving cytokine release syndrome, Cell Reports Medicine (2025), https://doi.org/10.1016/j.xcrm.2025.102531

STAR★METHODS

KEY RESOURCES TABLE

REAGENT or RESOURCE	SOURCE	IDENTIFIER
Antibodies		
APC-Cy7: mouse CD45	Biolegend	Cat# 103116; RRID:AB_312981
PE-Cy7: mouse CD3	eBbioscience	Cat# 25-0031-82; RRID:AB_469572
AF700:mouse B220	eBbioscience	Cat# 56-0452-82; RRID:AB_891458
PerCP-Cy5.5: mouse CD11b	eBbioscience	Cat# 45-0112-82; RRID:AB_953558
FITC: mouse Ly6C	BD	Cat# 561085; RRID:AB_10584332
PE: mouse Ly6G	BD	Cat# 551461; RRID:AB_394208
PE: mouse IL-6	Biolegend	Cat# 504504; RRID:AB_315338
PE-Cy7: human CD45	Biolegend	Cat# 304060; RRID:AB_2629599
APC: human CD19	Biolegend	Cat# 363006; RRID:AB_2564128
PerCP: human CD3	Biolegend	Cat# 300326; RRID:AB_2616610
RPLP0	Abcam	Cat# ab192866; RRID:AB_2814809
RPS3	Abcam	Cat# ab128995; RRID:AB_11145466
EIF2A	CST	Cat# 9722; RRID:AB_2230924
EIF4B	R&D	Cat# AF3800-SP; RRID:AB_2097540
Phospho-EIF4B (Ser422)	CST	Cat# 3591; RRID:AB_2097522
JAK1	CST	Cat# 50996; RRID:AB_2716281
NF-κB p65	CST	Cat# 4764; RRID:AB_823578
ERK1/2	CST	Cat# 9102; RRID:AB_330744
AKT	CST	Cat# 9272; RRID:AB_329827
Phospho-AKT	CST	Cat# 2965; RRID:AB_2255933
EIF4E	CST	Cat# 9742; RRID:AB_823488
p38 MAPK	CST	Cat# 9212; RRID:AB_330713
Phospho-RSK1 (S221)/RSK2 (S227)	R&D	Cat# AF892-SP; RRID:AB_2181317
RSK1/2/3	CST	Cat# 9355; RRID:AB_659900
Phospho-p70 S6 Kinase (T389)	CST	Cat# 9205; RRID:AB_330944
p70 S6 Kinase	CST	Cat# 2708; RRID:AB_390722
Phospho-4E-BP1 (T37/46)	CST	Cat# 9459; RRID:AB_330985
4E-BP1	CST	Cat# 9644; RRID:AB_2097841
Histone H3	CST	Cat# 9715; RRID:AB_331563
Donkey anti-goat IgG (H&L)-HRP conjugated antibody	Abcam	Cat# ab97110; RRID:AB_10679463
Goat anti-rabbit IgG (H&L)-HRP conjugated antibody	EASYBIO	Cat# BE0101; RRID:AB_3083002
Anti-puromycin fluorescent antibody-AF488	Millipore	Cat# MABE343-AF488; RRID:AB_2736875
Chemicals, peptides, and recombinant proteins		
Puromycin	Invivogen	Cat# ant-pr-1
Cycloheximide	Sigma	Cat# C7698
Human recombinant M-CSF	Peprotech	Cat# 300-25
LPS	Sigma	Cat# L4516
LJH685	MedChemExpress	Cat# HY-19712
Rapamycin	MedChemExpress	Cat# HY-10219
Wortmannin	MedChemExpress	Cat# HY-10197
GSK2334470	MedChemExpress	Cat# HY-14981

(*Continued on next page*)

Please cite this article in press as: Liu et al., Discovery, delineation, and therapeutic targeting of a hyper-translation pathway driving cytokine release syndrome, Cell Reports Medicine (2025), https://doi.org/10.1016/j.xcrm.2025.102531

Continued

REAGENT or RESOURCE	SOURCE	IDENTIFIER
GolgiStop	BD Biosciences	Cat# 554724
RNase inhibitor	Promega	Cat# N2511
Protease inhibitor cocktail	Bimake	Cat# B14001
RNase I	Invitrogen	Cat# AM2294
Critical commercial assays		
Human IL-6 ELISA MAX DELUXE	Biolegend	Cat# 430505
Mouse IL-6 ELISA Set	BD Pharmingen	Cat# 555240
Legendplex multi-analyte flow assay kit	Biolegend	Cat# 740621
NucleoSpin Blood XL kit	MACHEREY-NAGEL	Cat# 740950.50
RNeasy Mini kit	Qiagen	Cat# 74104
Deposited data		
BCAP KO vs. WT BMDM Ribo-seq	This paper	GEO: GSE287440
LPS stimulated vs. control BMDM Ribo-seq	This paper	GEO: GSE287441
BMDM RiboTag-seq	This paper	GEO: GSE287442
CRISPR screen	This paper	GEO: GSE287443
Human monocytes Ribo-seq	This paper	GEO: GSE287444
RSK1 KO BMDM RNA-seq	This paper	GEO: GSE287445
Experimental models: Organisms/strains		
Mouse *Pik3ap1*$^{fl/fl}$	Gempharmatech	T020059
Mouse *Rps6ka1*$^{-/-}$	Gempharmatech	T007518
Mouse *Lyz2*-Cre	Jackson Laboratories	IMSR_JAX:004781
Mouse NSG-SGM3	Jackson Laboratories	IMSR_JAX:013062
Mouse *Rpl22*$^{HA/HA}$	Jackson Laboratories	IMSR_JAX:029977
Mouse *Il6*$^{-/-}$	Jackson Laboratories	IMSR_JAX:002650
Mouse Cas9 transgenic	Jackson Laboratories	IMSR_JAX:026430
Software and algorithms		
Flowjo (v10.4)	Tree Star, Inc	N/A
Prism (v9.1.0)	GraphPad	N/A
ImageJ	ImageJ	N/A
Origin	Origin	N/A
MAGeCK	N/A	N/A
Microsoft Excel	Microsoft	N/A
Adobe Illustrator	Adobe	N/A
R	The R project	N/A
Other		
4–20% SDS-PAGE	Yeasen	Cat# 36231ES105
Anti-CD14 magnetic beads	Miltenyi	Cat# 130-050-201
EasySep Mouse CD90.2 Positive Selection Kit II	StemCell	Cat# 18951
Anti-HA beads	Thermo Fisher	Cat# 88836
HiScript III RT SuperMix	Vazyme	Cat# R323

EXPERIMENTAL MODEL AND STUDY PARTICIPANT DETAILS

Patient samples

Patients diagnosed with non-Hodgkin's lymphoma or multiple myeloma were treated at the Chinese PLA General Hospital (Beijing, China) and received CAR T infusion. Peripheral blood was collected pre- and post-CAR T (6–10 days) infusion followed by PBMC purification. This study was approved by the Ethics Committee of the Chinese PLA General Hospital. Informed consent was obtained from all patients.

Please cite this article in press as: Liu et al., Discovery, delineation, and therapeutic targeting of a hyper-translation pathway driving cytokine release syndrome, Cell Reports Medicine (2025), https://doi.org/10.1016/j.xcrm.2025.102531

Cells

B16-EGFR and Raji cell lines were cultured in RPMI 1640 medium (Corning, 10040CM) supplemented with 10% FBS (Gibco). These two cell lines are authenticated by specific antigen expression including EGFR and CD19, respectively. 293T and Plat-E cells were maintained in DMEM (Gibco, C11995500BT). Mycoplasma contamination is negative in all the cell lines used in this study. BMDMs were cultured in DMEM supplemented with 10% FBS and 10% supernatant from L929 mouse fibroblasts, which served as a source of macrophage colony stimulating factor (M-CSF). After 6 days of culture, floating cells were removed, and adherent macrophages were plated in multi-well plates overnight prior to stimulation. PBMCs from healthy donors were isolated from buffy coats (obtained from the Beijing Red Cross Blood Center) using density gradient centrifugation with Ficoll (STEMCELL Technologies, Lymphoprep). $CD14^+$ monocytes were further purified from PBMCs using anti-CD14 magnetic beads (Miltenyi Biotec, 130-050-201) and cultured in RPMI 1640 medium supplemented with 10% FBS (Gibco) and human recombinant M-CSF (Peprotech, 300-25; 10 ng/mL).

Mice

Pik3ap1$^{fl/fl}$ and *Rps6ka1*$^{-/-}$ mice on the C57BL/6J background were purchased from Gempharmatech. *Lyz2*-Cre and NSG-SGM3 mice were purchased from The Jackson Laboratories. *Pik3ap1*$^{fl/fl}$ mice were crossed with *Lyz2*-Cre mice to generate myeloid-specific BCAP knockout mice, using age and sex matched *Lyz2*$^{cre/cre}$ mice as control mice. Age and sex matched WT C57BL/6J mice were used as controls for *Rps6ka1*$^{-/-}$ mice. All the mice used in this study are 6–10 weeks old. *Rpl22*$^{HA/HA}$, *Il6*$^{-/-}$ and Cas9 transgenic mice were generously provided by Dr. Huabing Li, Dr. Wenwen Zeng and Dr. Min Peng, respectively. All mice were housed in individually ventilated cages in a temperature and light regulated room in a specific pathogen free facility and received food and water *ad libitum*. All animal procedures and experiments were performed in accordance with guidelines of the Laboratory Animal Research Center of Tsinghua University. The laboratory animal facility has been licensed by the Science and Technology Commission of Beijing Municipality (SYXK-2014-0024) and accredited by Association for Assessment and Accreditation of Laboratory Animal Care International. All animal protocols used in this study were approved by the Institutional Animal Care and Use Committee of Tsinghua University.

METHOD DETAILS

Virus packaging and transduction

293T cells were cultured in 10 cm dishes until they reached 80% confluence. The cells were then transfected using Opti-MEM medium containing 80 μL Lipofectamine 2000 mixed with the CAR plasmid (10 μg) and two packaging plasmids (pCMV-VSV-G, 7.5 μg; psPAX2, 5 μg). After 8 h, the medium was replaced with 8 mL of pre-warmed fresh medium, added gently to avoid disturbing the cells. The virus-containing supernatant was collected 24 h post-transfection, filtered through a 0.45 μm filter, aliquoted, and stored at −80°C for future use. For the CRISPR screen, the retroviral library was generated similarly using pCL-ECO and the library plasmid. The IL-6 overexpression retroviral vector was produced by transfecting the pMX-CMV plasmid into Plat-E cells. For BMDM viral infection, the virus was added to BMDMs on day 3 of differentiation, followed by replacement with fresh medium after 24 h.

Manufacture of CAR T cells and *in vitro* CAR T-mediated killing

The anti-CD19 CAR construct consists of a CD19 scFv fused in-frame with the hinge and transmembrane domains of CD8, followed by the cytoplasmic domains of CD28 and CD3ζ. To generate CAR T cells, PBMCs or cord blood mononuclear cells (CBMCs) from healthy donors were primed for 24 h with anti-CD3 (Biolegend, 300438) and anti-CD28 (BD, 555725) antibodies, followed by transduction with the CAR-expressing lentiviral vector for an additional 24 h. Transduced T cells were then replated and cultured in RPMI 1640 medium (Gibco, #C11875500BT) supplemented with 10% FBS (Gibco), 2 mM GlutaMAX (Gibco, #35050061), 10 mM HEPES, 1 mM sodium pyruvate, and IL-2 (Scintol, S10970015). To generate KS, the manufactured CAR T cells were co-cultured with Raji cells at an effector-to-target ratio of 2:1 for 48 h. The KS was collected via centrifugation and filtration, then mixed with RPMI medium at a 1:1 ratio for $CD14^+$ human monocyte stimulation.

For mouse CAR T cells, the anti-human EGFR CAR construct features an EGFR scFv fused in-frame with the hinge and transmembrane domains of CD8, followed by the cytoplasmic domains of CD28 and CD3ζ. T cells were isolated from the spleen and lymph nodes of WT C57BL/6J mice using the EasySep Mouse CD90.2 Positive Selection Kit II (StemCell, 18951). The isolated T cells were primed for 24 h with anti-CD3 (Liankebio, F2100300) and anti-CD28 (Liankebio, F2102800) antibodies, followed by transduction with the CAR-expressing lentiviral vector for an additional 24 h. To generate KS for mouse studies, the CAR T cells were co-cultured with B16-EGFR cells at an effector-to-target ratio of 1:1 for 48 h. The KS was collected via centrifugation and filtration, then mixed with DMEM medium at a 1:3 ratio for BMDM stimulation.

Flow cytometry and cell sorting experiments

Tissue was harvested from indicated mice and the red blood cells were lysed with ACK lysing buffer, and the cell suspensions were passed through a 70 μm cell strainer before being stained with antibodies for flow cytometry (CD45-APC-Cy7, Biolegend 103116; CD3-PE-Cy7 eBioscience 25-0031-82; B220-AF700 eBioscience 56-0452-82; CD11b-PerCP-Cy5.5 eBioscience #45-0112-82; Ly-6C-FITC BD 561085; Ly-6G-PE BD 551461). For humanized mice, peripheral blood cells were collected and stained for human markers (CD45-PE-Cy7, Biolegend, 304060; CD19-APC, Biolegend, 363006; CD3-PerCP, Biolegend, 300326). To measure viability,

cells were collected and stained with Annexin V Apoptosis Detection Kit FITC (eBioscience, 88-8005-72) according to the manufacturer's instructions. Flow cytometry assays were performed on FACSFortessa (BD Biosciences) and analyzed with FlowJo software.

Measurement of cytokines

Culture supernatants and serum samples were collected after centrifugation at 5,000 rpm for 5 min and stored at −80°C. For newly synthesized IL-6 measurements, cells were treated by GolgiStop (BD Biosciences, 554724) for 4 h and then lysed by RIPA. Human IL-6 was measured by IL-6 ELISA MAX Deluxe (BioLegend, 430505) and mouse IL-6 was measured by Mouse IL-6 ELISA Set (BD Pharmingen, 555240) according to manufacturers' instructions. Mouse IFN-γ, TNF-α, and IL-1β were measured by Legendplex multi-analyte flow assay kit (Biolegend, 740621).

RNA extraction and quantitative PCR

Total RNA was extracted from cells using Trizol reagent, and was reverse-transcribed to complementary DNA (cDNA) using HiScript III RT SuperMix (Vazyme, R323). Real-time PCR was done in triplicate with SYBR Green Master Mix (Applied Biosystems, A25742) and a 7500 Real-time PCR system (Applied Biosystems). Primers for human transcripts were as follows (forward primer, reverse primer, listed as 5′ > 3′): *GAPDH*: TTCGACAGTCAGCCGCATC GCCCAATACGACCAAATCCG; *IL6*: TGGCAGAAAACAACCTG AACC CCAGTGATGATTTTCACCAGGC. Mouse transcripts: *Gapdh*: AGGTCGGTGTGAACGGATTTG GGGGTCGTTGATGGCA ACA; *Il6*: TCTATACCACTTCACAAGTCGGA GAATTGCCATTGCACAACTCTTT.

Western blotting

Cells were lysed by RIPA (Beyotime, P0013B) and protein lysates were denatured at 95°C for 6 min. Denatured cell lysates were separated by 4–20% SDS-PAGE (Yeasen, 36231ES105) and transferred to a PVDF membrane (Millipore) by electroblotting. Membranes were blocked in 2.5% BSA dissolved in TBST at room temperature for 1 h and incubated at 4°C overnight with the following 1:1000 diluted primary antibodies in 2.5% BSA dissolved in TBST buffer: RPLP0 (Abcam, ab192866), RPS3 (Abcam, ab128995), EIF2A (CST, 9722), EIF4B (R&D, AF3800-SP), Phospho-EIF4B (Ser422) (CST, 3591), JAK1 (CST, 50996), NF-κB p65 (CST, 4764), ERK1/2 (CST, 9102), Phospho-AKT (CST, 2965), AKT (CST, 9272), p38 MAPK (CST, 9212), Phospho-RSK1 (S221)/RSK2 (S227) (R&D, AF892-SP), RSK1/2/3 (CST, 9355), Phospho-p70 S6 Kinase (Thr389) (CST, 9205), p70 S6 Kinase (CST, 2708), Phospho-4E-BP1 (Thr37/46) (CST, 9459), 4E-BP1 (CST, 9644), Histone H3 (CST, 9715). The membranes were then washed and incubated with goat anti-rabbit IgG (H&L)-HRP conjugated antibody (EASYBIO, BE0101) or donkey anti-goat IgG (H&L)-HRP conjugated antibody (Abcam, ab97110) for 1 h at room temperature. Proteins were visualized using SuperSignal West Pico Chemiluminescent Substrate (Thermo Fisher Scientific, 34080) and captured with the ImageQuant LAS 400 imaging system (GE Healthcare Life Sciences).

Mass spectrometry data collection and analysis

Protein samples lysed from patient-derived PBMCs were separated on SDS-PAGE. The corresponding gel lane was excised, reduced with 10 mM of TCEP, and alkylated with 40 mM chloroacetamide. Mass spectrometry data acquisition and analysis were accomplished by Technology Center for Protein Sciences, Tsinghua University.

Surface sensing of translation (SUnSET) assay

The SUnSET assay was employed to assess mRNA translation rates by quantifying puromycin incorporation. Cells were treated with 1 μg/mL puromycin (Invivogen, ant-pr-1) and incubated for 30 min at 37°C. Subsequently, the cells were processed for cytospin slide preparation. The samples were fixed with 4% paraformaldehyde (Sigma, 158127) and stained with an anti-puromycin fluorescent antibody (Sigma, MABE343-AF488). Puromycin incorporation was visualized using confocal microscopy, and the translation rate, reflected by puromycin fluorescence intensity, was quantified using ImageJ software.

Polysome profiling

Following treatment with 100 μg/mL cycloheximide (Sigma, C7698), cells were washed with ice-cold PBS and pelleted by centrifugation. Cell pellets were resuspended in polysome lysis buffer (20 mM Tris-HCl [pH 8.0], 140 mM NaCl, 15 mM $MgCl_2$, 100 μg/mL cycloheximide, 1 mM DTT, 0.5% Triton X-100) supplemented with protease inhibitor cocktail (Bimake, B14001) and RNase inhibitor (Promega, N2511). Homogenization was achieved through five to six passages through a 26-gauge needle using a 1 mL syringe. The clarified lysates were carefully layered onto preformed 10%–50% linear sucrose density gradients prepared in polysome buffer. Gradients were subjected to centrifugation at 35,000 rpm for 2 h using an SW41 rotor in a Beckman ultracentrifuge. The Gradient fractionation system (ISCO Model 160 Gradient Former Foxy Jr. Fraction Collector) was used to isolate sucrose gradient fractions. The abundance of ribosomal RNA was measured by monitoring the absorbance at 260 nm.

Ribosome profiling (Ribo-seq) library preparation, sequencing and data analysis

Cells pellets were lysed with polysome lysis buffer and cell lysate was digested with RNase I (Invitrogen, AM2294) to generate RPF which is subjected to conventional Ribo-seq library construction.[24] A portion of the cells were used for RNA-seq. The RPF libraries were pooled and sequenced on an HiSeq X Ten platform and 150 bp paired-end reads were generated. The sequencing was performed by Genewiz Technology Co., Ltd. Raw sequencing data were processed by Tsinghua Bioinformatic Platform, which included

fastq_quality_filter (v0.0.14) for quality control, cutadapt (v2.8) for adapter trimming, bowtie2 (v1.3.1) for rRNA alignment and STAR (v2.7.10a) for genome (GRCh38/GRCm38) mapping. For TE Calculation: TE = (RPF/mRNA counts) × 1e6. Genes with RPF ≥1 RPM and |log2(TE_experiment_group/TE_control_group)| > 1 (FDR <0.05, DESeq2) were deemed differentially translated. For GO analysis, clusterProfiler (v4.6.2) was employed with hypergeometric test by Benjamini-Hochberg FDR correction.

RNA-seq and data analysis

Total RNA was extracted with Trizol reagent and was submitted for RNA-seq. Sequencing libraries were generated using NEBNext Ultra RNA Library Prep Kit for Illumina according to the manufacturer's instructions. Quality control of libraries was performed with the Agilent 2100 bioanalyzer instrument. High-throughput sequencing was performed using the Illumina Novaseq 6000 platform and 150 bp paired-end reads were generated. Softwares including TrimGalore (v0.6.7), HISAT2 (v2.2.1), featureCounts (v2.0.3) were employed for reads processing and FPKM was calculated for expression (FDR< 0.01 (edgeR)).

RiboTag-seq library preparation, sequencing and data analysis

Cells were homogenized and then centrifuged at 10,000g for 10 min. Supernatants were added directly to the anti-HA beads (Thermo Fisher, 88836) and rotated for 6 h at 4°C. A portion of the supernatant was kept as input samples for bulk RNA-seq. Following rotation, samples were placed in a magnet on ice. The supernatants were recovered, and the pellets three times for 5 min in high salt buffer. To isolated RiboTagged transcripts and bulk mRNA, Qiagen RLT buffer (part of the RNeasy Mini kit, Qiagen, 74104) was added to the remaining pellets or to the input samples, respectively. Total RNA was extracted following the manufacturer's instructions using the RNeasy Mini kit. Purified RiboTagged transcripts and bulk mRNA were subjected to RNA-seq analysis. Data processing included fastq_quality_filter (v0.0.14) for quality control, cutadapt (v2.8) for adapter trimming, bowtie2 (v1.3.1) for rRNA alignment and STAR (v2.7.10a) for genome (GRCh38/GRCm38) mapping. For TE Calculation: TE = (RiboTagged transcripts counts/mRNA counts) × 1e6. Genes with RiboTagged transcripts ≥1 and |log2(TE_experiment_group/TE_control_group)| > 1 (FDR <0.05, DESeq2) were deemed differentially translated.

Patient samples

Patients diagnosed with non-Hodgkin's lymphoma or multiple myeloma were treated at the Chinese PLA General Hospital (Beijing, China) and received CAR T infusion. Peripheral blood was collected pre- and post-CAR T (6–10 days) infusion followed by PBMC purification. This study was approved by the Ethics Committee of the Chinese PLA General Hospital. Informed consent was obtained from all patients.

CRISPR screen and data analysis

Cas9-transgenic BMDMs were cultured and transduced with a macrophage-specific retroviral library with sgRNAs of 2425 macrophage-expressing genes (4 sgRNAs per gene) on day 3 differentiation at an infection rate of approximately 30%. After 24 h, the medium was replaced with fresh M-CSF-containing medium. By day six, library infected GFP positive BMDMs were sorted and cultured for an additional two days. The cells were then divided into an experimental group with KS stimulation and a control group as input. Following 72 h of stimulation, cells were treated with GolgiStop for 4 h and collected for intracellular staining by IL-6 fluorescent antibody (Biolegend, 504504). The bottom 5% of IL-6-expressing cells were sorted, and genomic DNA was extracted from both the sorted cells and unstimulated control group using the NucleoSpin Blood XL kit (MACHEREY-NAGEL, 740950.50). The sgRNA cassettes were amplified by PCR according to the broad GPP protocol and subsequently subjected to deep sequencing. For data analysis, the MaGeCK tool (v0.5.9.4) was used to process and analyze the CRISPR screen sequencing data. Fastq reads were processed using the count module, and the RRA module (default setting) was used to calculate $\log_2$ fold changes and p-values of the genes. Data visualization was performed using Custom R scripts (v4.1.3).

Construction of humanized mouse model

Humanized mice were generated from triple transgenic NSG-SGM3 mice (6–8 weeks old) expressing human signal regulatory protein alpha (SIRPα), granulocyte-macrophage colony-stimulating factor (GM-CSF), interleukin-3 (IL-3), and stem cell factor (SCF). Each mouse was subjected to 1.3Gy irradiation and immediately intravenously (*i.v.*) injected with 0.08 million human cord blood-derived $CD34^+$ HSC (purchased from Bairuikang Biotechnology). To construct CRS model, 0.5 million Raji cells were *i.v.* injected into each mouse 6 weeks after human immune reconstruction. Two weeks later, 5 million anti-CD19 CAR T cells generated from CBMCs of same HSC donors were *i.v.* injected into each mouse. At indicated time points, 20mg/mL LJH685 was *i.p.* administered. Blood samples were collected to measure IL-6 levels and quantify tumor cells and CAR T cells. For tissue analysis, mice were deeply anesthetized with Avertin and perfused intracardially with ice-cold PBS, followed by 4% PFA. Organs were dissected, post-fixed overnight in 4% PFA at 4°C, Heart, liver and spleen were sent for paraffin embedding and H&E staining.

QUANTIFICATION AND STATISTICAL ANALYSIS

GraphPad Prism software was used for data analysis. Types of statistical tests are indicated in figure legends. For graphs, data are shown as mean ± SEM; $^*p < 0.05$, $^{**}p < 0.01$, $^{***}p < 0.001$, $^{****}p < 0.0001$, ns, not significant.